THE ASTROPHYSICAL JOURNAL, 258:335–348, 1982 July 1

ELECTRON-POSITRON PAIR EQUILIBRIA IN RELATIVISTIC PLASMAS[1]

ROLAND SVENSSON
Lick Observatory, Board of Studies in Astronomy and Astrophysics, University of California at Santa Cruz
Received 1981 September 24; accepted 1982 January 8

ABSTRACT

The physical properties of a thermal plasma of size R in the temperature range θ ($\equiv kT/mc^2$, where m is the electron mass) $= \frac{1}{3}$–100 are studied assuming pair equilibrium and thermal balance. The radiation field is obtained by multiplying the spectral emissivities by the photon escape time. The effect of scatterings is approximately allowed for by treating them as coherent. All important pair and photon producing processes in a plasma with a Thomson scattering optical depth τ_T of order unity or less are included. The spectral emissivities and the cooling rates for bremsstrahlung and pair annihilation are discussed. The photon-photon, photon-particle, and particle-particle pair production rates, and the pair annihilation rate as well as the opacities are calculated. Simple approximate expressions are given for several rates.

The equilibrium ratio z of the pair density n_+ to the proton density N is given by the roots to the pair equilibrium equation (a polynomial in z). For a given $\tau_N \equiv Nr_e^2R < 10^{-1}$, there exists a temperature θ_c beyond which the pair annihilation rate cannot balance the pair production rate and there are no pair equilibria. For $\theta < \theta_c$ there are a high-z pair equilibrium branch ($z \gg 1$) with τ_T of order unity, where photon-photon pair production dominates, and an optically thin low-z pair equilibrium branch ($z \ll \tau_N^{-1}$), where particle-particle pair production dominates. The temperature θ_c has a maximum value $\theta_{\max} \approx 25$ for $\tau_N \lesssim 10^{-4}$ and decreases monotonically for larger τ_N. Several aspects of the obtained pair equilibria, such as parameter space dependence, cooling rates, optical depths, stability, and confinement are briefly discussed.

Optically thick ($\tau_T > 1$) pair equilibria are considered qualitatively. The approach of the solution curves in the z-θ plane to complete thermodynamic equilibrium is expected to occur at a temperature $\theta_{\min} \approx \frac{1}{10}$–$\frac{1}{3}$. The physical significance of $\theta_{\min}$ and $\theta_{\max}$ is discussed.

A pair *equilibrium* plasma is kept at $\theta_{\min}$ (for $\tau_T > 1$) or at $\theta_{\max}$ (for $\tau_T < 10^{-3}$) over a wide range of heating rates. It is, however, emphasized that realistic semirelativistic plasmas may be neither in pair equilibrium nor in thermal balance.

Subject headings: gamma rays: general — opacities — plasmas — radiation mechanisms — relativity

I. INTRODUCTION

The physical processes, the heating and cooling mechanisms, the thermal equilibria, and the ionization equilibria occurring in tenuous astrophysical plasmas at temperatures $\theta \equiv kT/mc^2 < 10^{-2}$ (where k is the Boltzmann constant, m the electron mass, and c the speed of light) are reasonably well understood. However, observations of gamma-ray emission from a wide variety of objects, such as gamma-ray bursts (most likely originating from neutron stars; Mazets *et al.* 1981), the Seyfert galaxy NGC 4151 (Baity *et al.* 1981), and the quasar 3C 273 (Bignami *et al.* 1981), indicate that astrophysical plasmas may achieve semirelativistic or relativistic temperatures. At semirelativistic temperatures a number of threshold processes appear, associated with creation of electron-positron pairs. The pairs are produced through photon-photon, photon-particle, and particle-particle interactions. The created pairs either annihilate into photons or participate in other photon and pair producing processes. In a steady state situation at a given temperature (i.e., assuming thermal balance), the radiation field and the pair density must be determined simultaneously by solving a nonlinear radiative transfer equation (with the nonlinearity introduced through photon-photon absorption) and a pair equilibrium equation (balancing the pair production and pair annihilation rates).

Very little is known about the equilibrium properties of a semirelativistic or relativistic plasma. Bisnovatyi-Kogan, Zel'dovich, and Sunyaev (1971, hereafter BK) considered a relativistic ($\theta \gg 1$) plasma in the limit where the photon density is so small that only pair production by particle-particle collisions is important. The equilibrium pair density was found to increase with temperatures until $\theta \approx 40$, where the equilibrium pair density approaches infinity. At higher temperatures no pair equilibrium is possible. BK also derived an approximate expression for the pair density at nonrelativistic temperatures ($\theta \ll 1$). Stoeger (1977) treated the case where photon-photon pair production is important. The equilibrium pair density in the temperature range

[1] *Lick Observatory Bulletin*, No. 910.

$\frac{2}{3} \leq \theta \leq 1$ was found to be much smaller than the proton density of the medium. In fact, the obtained pair densities are much smaller than an interpolation of BK's results between low and high temperatures. This is inconsistent since BK's solution describes the minimum equilibrium pair density. Inclusion of photon processes should raise the pair density at a given temperature. Also, a closer study of Stoeger's pair equilibrium equation reveals a second solution (not explored by Stoeger), where the equilibrium pair density is larger than the background proton density.

We extend the above work by including most of the important processes influencing the equilibrium properties of a plasma in the temperature range $\frac{1}{3} < \theta < 100$. It is assumed that Comptonization and absorption processes have little or negligible effect on the radiation field. The included processes are treated as exactly as possible, i.e., the exact cross sections are used when available, and the rates are calculated, taking into account all relativistic kinematic effects.

In § II the model is presented and the validity of the adopted assumptions is discussed. The radiation processes are treated in § III, and the corresponding cooling rates in § IV. Pair production rates, annihilation rates, and opacity coefficients are calculated in § V. The properties of the solutions to the pair equilibrium equation are discussed and compared to other work in § VI. Section VII treats qualitative aspects of a plasma with a Thomson scattering optical depth larger than unity. Section VIII contains a discussion of some general implications of the obtained results as well as a summary of possible pair equilibria.

Finally, it should be emphasized that it is not the intention of this work to model realistic, semirelativistic plasmas, but rather to explore the properties of semirelativistic plasmas using certain simplifying assumptions. The results of this paper will form a point of departure for forthcoming work, where some of these assumptions are relaxed.

II. THE MODEL

Consider a stationary, uniform, neutral plasma of size R consisting of protons (p), electrons (e^-), positrons (e^+) and photons (γ) with densities N, n_-, n_+, and $n(x)dx$, respectively. The quantity $n(x)dx$ represents the density of photons with energy x (expressed in units of mc^2) in the energy interval dx. The charge neutrality condition reads

$$n_- = N + n_+ \,. \tag{1}$$

All quantum electrodynamical processes to order α^3 in the coupling constant (the fine-structure constant) occurring in such a plasma are listed in Table 1. Also listed are the lowest order (α^4) particle-particle pair production processes, important only when the photon density is small.

The Lorentz factors γ of the electrons and positrons are assumed to have a relativistic Maxwell-Boltzmann distribution,

$$f(\gamma)d\gamma = [\theta K_2(1/\theta)]^{-1}\beta\gamma^2 \exp(-\gamma/\theta)\,, \tag{2}$$

TABLE 1

PHYSICAL PROCESSES IN RELATIVISTIC PLASMAS

Basic Two Body Interaction	Radiative Variant	Pair Producing Variant
Møller and Bhaba scattering $ee \rightarrow ee$	Bremsstrahlung $ee \leftrightarrow ee\gamma$	$ee \leftrightarrow eee^+e^-$
Compton scattering $\gamma e \rightarrow \gamma e$	Double Compton scattering $\gamma e \leftrightarrow \gamma e\gamma$	$\gamma e \leftrightarrow ee^+e^-$
Pair annihilation $e^+e^- \rightarrow \gamma\gamma$	Three quantum annihilation $e^+e^- \leftrightarrow \gamma\gamma\gamma$	...
Photon-photon pair production $\gamma\gamma \rightarrow e^+e^-$	Radiative pair production $\gamma\gamma \leftrightarrow e^+e^-\gamma$	...
Processes Involving Protons		
Coulomb scattering $ep \rightarrow ep$	Bremsstrahlung $ep \leftrightarrow ep\gamma$	$ep \leftrightarrow epe^+e^-$ $\gamma p \leftrightarrow pe^+e^-$

characterized by the dimensionless temperature parameter

$$\theta \equiv kT/mc^2 \,. \tag{3}$$

$K_n(x)$ is the modified Bessel function of second kind of order n, and $\beta = (\gamma^2 - 1)^{1/2}/\gamma$. Gould (1981*b*, 1982) did a detailed investigation of the relaxation time scales in a relativistic plasma and found that Møller ($e^{\pm}e^{\pm}$) and Bhaba (e^+e^-) scatterings cannot maintain a Maxwellian electron and positron distribution for $\theta > 3.5$. At higher temperatures bremsstrahlung losses dominate the relaxation processes, and deviations in the Maxwellian tail occur. In the temperature range where we find equilibrium solutions ($\theta < 25$), the deviations are not appreciable and our results are still applicable, as long as θ represents the mean energy of the particles.

For temperatures considered here, the protons have a nonrelativistic Maxwell-Boltzmann distribution and can be viewed as being at rest.

All pair producing and photon producing processes listed in Table 1 are included in the model, except double Compton scattering, radiative pair production, three quantum annihilation, and any applicable three or four body process. Some excluded processes as well as absorption processes are of marginal importance for certain equilibrium solutions. For these solutions the Thomson scattering optical depth of the medium,

$$\tau_T = (n_+ + n_-)\frac{8\pi}{3} r_e^2 R \,, \tag{4}$$

is of order unity (r_e is the classical electron radius).

If the optical thickness to absorption processes is small at photon energies of interest, then the photon density at energy x in the medium can be written as

$$n(x) \approx \dot{n}(x) t_{\rm esc}(x) \,, \tag{5}$$

where $\dot{n}(x)dx$ ergs cm^{-3} s^{-1} is the production rate of photons of energy x in the energy interval dx, and t_{esc} is the photon escape time of the medium. As τ_T is of order unity in some cases, Comptonization and spatial diffusion should be taken into account. Comptonization is neglected, but its influence on the solutions is shown to be not very large. As it turns out that spatial diffusion becomes important only at temperatures $\theta \lesssim 6$, it is treated in the Thomson limit by simply taking into account the prolonged pathway due to scatterings during photon escape (see, e.g., Rybicki and Lightman 1979),

$$t_{esc} \approx \frac{R}{c}(1 + \tau_T) . \quad (6)$$

The sensitivity of the results to spatial diffusion is tested by excluding the enhancement factor $(1 + \tau_T)$.

The radiation field is treated both as homogeneous and isotropic (cf. eq. [5]). This is a gross approximation of the true situation, where the radiation field is non-isotropic and inhomogeneous and extends beyond the plasma region of interest, producing a halo of pairs. The inhomogeneous problem as well as the inclusion of neglected but marginally important processes are deferred to future studies.

Two useful dimensionless quantities are introduced. The pair density is expressed in units of the proton density,

$$z \equiv \frac{n_+}{N} , \quad (7)$$

and the size, R, and the proton density, N, are combined to form the parameter

$$\tau_N \equiv N r_e^2 R . \quad (8)$$

Equation (4) can be rewritten in terms of z and τ_N, using equation (1), as

$$\tau_T = \frac{8\pi}{3}\tau_N(1 + 2z) . \quad (9)$$

III. THE RADIATION FIELD

The photon generating processes treated here are pair annihilation and bremsstrahlung. In a plasma consisting of electrons, positrons, and protons there are four different types of bremsstrahlung, namely, e^-p, e^+p, $e^\pm e^\pm$, and e^+e^-. In the Born approximation the e^-p and e^+p cases are identical (e.g., Jauch and Rohrlich 1976) and only three cases need to be considered. The total radiation field, $n(x)$ cm^{-3}, can be written as

$$n(x) = n_A(x) + n_{ep}(x) + n_{ee}(x) + n_{+-}(x) , \quad (10)$$

where $n_A(x)$, $n_{ep}(x)$, $n_{ee}(x)$, and $n_{+-}(x)$ are the photon densities at energy x due to pair annihilation and bremsstrahlung from ep, $e^\pm e^\pm$, and e^+e^- interactions, respectively. Using equations (1) and (5)–(8) and the dependence on density of the emissivities, equation (10) is rewritten as

$$n(x) \equiv N\tau_N(1 + \tau_T)[(z + z^2)S_A + (1 + 2z)S_{ep} + (1 + 2z + 2z^2)S_{ee} + (z + z^2)S_{+-}] , \quad (11)$$

which defines the spectral shape functions $S_i(x, \theta)$ (where i symbolizes one of the four radiation mechanisms).

In this section analytical expressions for $S_i(x, \theta)$ are found. Maxon (1972) employed an interpolation procedure to determine the bremsstrahlung spectra at semi-relativistic temperatures, knowing the spectra analytically at nonrelativistic and extreme relativistic temperatures. Here, instead, simple correction functions are applied to the analytical expressions.

a) *The Pair Annihilation Spectrum*

The pair annihilation process in a thermal plasma and its resulting spectrum have been discussed by Zdziarski (1980), Ramaty and Mészáros (1981), and Svensson (1982).

At nonrelativistic temperatures, the slightly Doppler-broadened annihilation spectrum peaks at photon energy $x = 1$. At semirelativistic temperatures, the kinetic energy of the annihilating particles becomes important and the spectral peak moves to higher energies and is broadened. As no simple analytical expression for the spectrum exists in this regime, the numerical fit that Zdziarski (1980) made to his Monte Carlo calculations is used for $\theta < 4$. At temperatures $\theta > 4$ the simple expression

$$S_A(x, \theta) = \frac{\pi}{2\theta^4}(\ln 4\eta\theta x - 1)x \exp(-x/\theta) , \quad (12)$$

obtained by Svensson (1982), is used. The constant η is defined as $\eta \equiv \exp(-\gamma_E) = 0.5616$, where $\gamma_E \approx 0.5772$ is Euler's constant.

The cooling rate obtained by integrating the chosen spectrum over $n_+ n_- cr_e^2 mc^2 x dx$ deviates from the exact pair annihilation cooling rate (see § IV) by at most 10%.

b) *ep Bremsstrahlung*

The spectrum $S_{ep}(x, \theta)$ of photons emitted by thermal electrons and positrons decelerating in the fields of protons is obtained by averaging the Bethe-Heitler cross section $d\sigma/dx$ (Jauch and Rohrlich 1976) over the Maxwell-Boltzmann distribution $f(\gamma)d\gamma$ (eq. [2]) of the electrons and positrons,

$$S_{ep}(x, \theta) = \int_{1+x}^{\infty} d\gamma f(\gamma)\beta\left(\frac{d\sigma}{dx}(x, \gamma)/r_e^2\right) . \quad (13)$$

Equation (13) has been integrated analytically in the relativistic limit, $x \gg 1$ and $\theta \gg 1$, by Quigg (1968) and in the nonrelativistic limit, $x \ll 1$ and $\theta \ll 1$, by Frank-Kamenetskii (1962). These asymptotic results are grossly in error at $\theta \approx 1$.

For $\theta \geq 1$, we replace the logarithmic factor $\ln[2\gamma(\gamma - x)/x]$ in the relativistic limit of the Bethe-Heitler cross section with $\beta^{-2} \ln[2(\gamma - 1)(\gamma - x)/x]$. For a given photon energy x, the resulting cross section better approximates the exact cross section near the threshold $\gamma_t = 1 + x$ then does the relativistic expression. Furthermore, equation (13) can be integrated analytically, and the resulting, rather complex expression agrees with a numerical determination of the exact spectrum to within 6% at $\theta = 1$, while becoming increasingly accurate at higher temperatures.

For $\theta \leq 1$ it is convenient to use the result of Gluckstern, Hull, and Breit as quoted by Kylafis and Lamb (1982), where higher order terms in θ and x to the nonrelativistic dipole spectrum are given. This expression breaks down for $x > 1$, the energy range of interest in pair producing processes. A correction factor is applied, making the deviations from an exact numerical integration of equation (13) less than 7% for $\theta \leq 1$ and $x < 10^2$.

c) $e^{\pm}e^{\pm}$ *Bremsstrahlung*

At relativistic temperatures, $\theta \geq 1$, the spectrum calculated by Alexanian (1968) is used. During relativistic $e^{\pm}e^{\pm}$ collisions both particles can be thought of as radiating, giving a spectrum about twice as large as for *ep* collisions, where only one of the interacting particles radiates. Furthermore, the relative Lorentz factor, γ_R, is of order $2\gamma_1\gamma_2$ for $e^{\pm}e^{\pm}$ collisions, while simply being equal to γ for *ep* collisions (γ_1, γ_2, and γ are Lorentz factors in the observer's frame for the radiating particles). As γ_R appears in the leading logarithmic term in the extreme relativistic cross section, the large relative Lorentz factor in the $e^{\pm}e^{\pm}$ case introduces an additional factor of 2 when averaging over the particle distributions. Finally, a factor of $\frac{1}{2}$ occurs as the interacting particles are identical. The $e^{\pm}e^{\pm}$ spectrum is therefore expected to be approximately $2 \times 2 \times \frac{1}{2}$ times as large as the *ep* spectrum in the extreme relativistic limit. In fact, this is seen explicitly by comparing the cooling functions for the two cases (see § IV).

At nonrelativistic temperatures, $\theta \leq 1$, and for photon energies, $x < 1$, the quadrupole spectrum calculated by Gould (1980, 1981*a*) is used. A correction factor, $1 + \theta$, is applied to bring Gould's spectrum into approximate agreement (to within 30%) with the relativistic spectrum at $\theta = 1$. For $x > 1$ the radiating particle must be relativistic, while the other particle typically is nonrelativistic. If so, the high energy ($x > 1$) part of the $e^{\pm}e^{\pm}$ spectrum per pair of particles should be approximately equal to the corresponding *ep* spectrum at nonrelativistic temperatures, while becoming 4 times larger at relativistic temperatures, as discussed above. Taking into account the identity of the particles, the *ep* spectrum multiplied with a correction factor $(1 + 3\theta)/2$ is used to describe the $e^{\pm}e^{\pm}$ spectrum for $\theta \leq 1$ and $x > 1$. The resulting spectrum agrees to within 25% with the relativistic spectrum at $\theta = 1$.

The cooling rate calculated using the chosen spectrum deviates by less than 6% from the cooling rate in § IV in the semirelativistic regime, while becoming very accurate at $\theta \ll 1$ and $\theta \gg 1$.

d) $e^{+}e^{-}$ *Bremsstrahlung*

At relativistic temperatures, $\theta \geq 1$, the result by Alexanian (1968) is used. The $e^{\pm}e^{\pm}$ cross section he employs is essentially identical to the $e^{+}e^{-}$ cross section except in the high-frequency limit, $\gamma - x \ll 1$ (Baĭer, Fadin, and Kroze 1968). This difference becomes negligible when the cross section is averaged over the particle distributions. The relativistic $e^{+}e^{-}$ spectrum is about 4 times larger than the relativistic *ep* spectrum (cf. § III*c*).

At nonrelativistic velocities the process, as viewed in the center-of-momentum (CM) frame, can be reduced to the equivalent one-body problem (i.e., the *ep* case), where a particle with reduced mass $m/2$ moving at relative velocity $2\beta_{CM}$ radiates in the field of an infinitely heavy particle. In fact, the cross section in the CM frame is just the nonrelativistic limit of the Bethe-Heitler cross section (Joseph and Rohrlich 1958). After averaging the cross section over a relative nonrelativistic Maxwell-Boltzmann distribution, the $e^{+}e^{-}$ spectrum for $\theta \ll 1$ and $x \ll 1$ is found to be $2^{3/2}$ larger than the *ep* spectrum. This result is most easily obtained by replacing the mass m in the expression for the *ep* spectrum with the reduced mass $m/2$. The $e^{+}e^{-}$ spectrum at $\theta \ll 1$ and $x \gg 1$ is equal to the corresponding *ep* spectrum. To describe the $e^{+}e^{-}$ spectrum for $\theta \leq 1$, a simple correction function of θ and x, having the limits stated above, is applied to the *ep* spectrum, so that the difference at $\theta = 1$ as compared with the relativistic spectrum is less than 30%.

IV. COOLING RATES

The cooling rate, Λ_A ergs cm^{-3} s^{-1}, for thermal pair annihilation was given as a single integral by Zdziarski (1980). The nonrelativistic cooling rate,

$$\Lambda_A = n_+ n_- cr_e^2 mc^2 2\pi \quad (\alpha^2 \ll \theta \ll 1)\,, \tag{14}$$

can be combined with the relativistic cooling rate obtained by Svensson (1982),

$$\Lambda_A = n_+ n_- cr_e^2 mc^2 \frac{2\pi}{\theta}(\ln 2\eta\theta + \tfrac{1}{4}) \quad (\theta \gg 1)\,, \tag{15}$$

to form the expression

$$\Lambda_A = n_+ n_- cr_e^2 mc^2 \frac{2\pi}{1/(1+6\theta) + \theta/[\ln(2\eta\theta+1) + \frac{1}{4}]} \quad (\theta \gg \alpha^2)\,, \tag{16}$$

which agrees to within 2% with a numerical evaluation of Zdziarski's integral.

Stickforth (1961) gave the cooling rate, Λ_{ep}, for thermal *ep* bremsstrahlung both as a single integral and as an approximate but rather complicated expression. By applying instead simple correction factors to the nonrelativistic cooling rate (e.g., Stickforth 1961) and the relativistic cooling rate (Stickforth 1961), the following expressions,

$$\Lambda_{ep} = (n_+ + n_-)Ncr_e^2 mc^2 \alpha \frac{32}{3}\left(\frac{2\theta}{\pi}\right)^{1/2}(1 + 1.781\theta^{1.34}) \quad (\alpha^2 \ll \theta \leq 1) \tag{17}$$

and

$$\Lambda_{ep} = (n_+ + n_-)Ncr_e^2 mc^2 \alpha 12\theta[\ln(2\eta\theta + 0.42) + \tfrac{3}{2}] \quad (\theta \geq 1)\,, \tag{18}$$

were found to deviate by less than 2% from the exact cooling rate.

Haug (1975*b*) wrote the thermal $e^{\pm}e^{\pm}$ bremsstrahlung rate, Λ_{ee}, as a double integral over an approximate (to within 6%) integrand. Applying a correction factor to the nonrelativistic quadrupole rate (Stickforth 1961),

$$\Lambda_{ee} = (n_+^2 + n_-^2) c r_e^2 m c^2 \alpha \frac{20}{9(\pi)^{1/2}} (44 - 3\pi^2)\theta^{3/2} \times (1 + 1.1\theta + \theta^2 - 1.25\theta^{2.5}) \quad (\alpha^2 \ll \theta < 1), \tag{19}$$

and using the relativistic cooling rate (Alexanian 1968),

$$\Lambda_{ee} = (n_+^2 + n_-^2) c r_e^2 m c^2 \alpha 24\theta(\ln 2\eta\theta + \tfrac{5}{4}) \quad (\theta \geq 1), \tag{20}$$

it is found that the deviations from a numerical evaluation of Haug's double integral is less than 2%.

The cooling rate, Λ_{+-}, for thermal e^+e^- bremsstrahlung has not yet been treated in the literature. From the arguments made in § III*d*, the nonrelativistic e^+e^- cooling rate is expected to be larger than the nonrelativistic *ep* cooling rate by a factor of $2^{3/2}$. In the relativistic limit, Alexanian's (1968) $e^{\pm}e^{\pm}$ result is expected to be valid (after multiplying by a factor of 2, as the particles are nonidentical). The following expressions,

$$\Lambda_{+-} = n_+ n_- c r_e^2 m c^2 \alpha 2^{3/2} \frac{32}{3}\left(\frac{2\theta}{\pi}\right)^{1/2}(1 + 1.7\theta^{1.5}) \quad (\alpha^2 \ll \theta < 1) \tag{21}$$

and

$$\Lambda_{+-} = n_+ n_- c r_e^2 m c^2 \alpha 48\theta(\ln 2\eta\theta + \tfrac{5}{4}) \quad (\theta \geq 1), \tag{22}$$

agree to within 4% with the cooling rate obtained by numerically integrating the spectrum chosen in § III*d*.

The four cooling rates are shown in Figure 1. It is concluded that in an optically thin plasma the total bremsstrahlung cooling always dominates the annihilation cooling for temperatures $\theta > 3.5$, independent of the number of pairs present. In plasmas that are at least marginally optically thick to Thomson scattering, Comptonization will amplify the bremsstrahlung cooling, extending its dominance in pair plasmas to even lower temperatures.

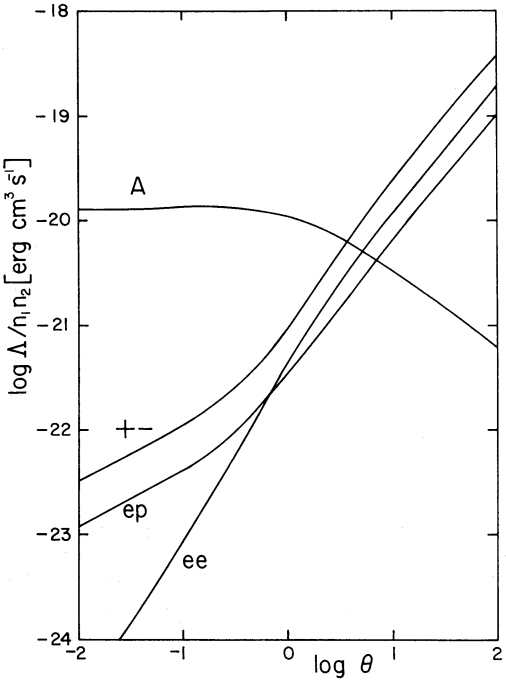

FIG. 1.—The total power emitted per unit volume, Λ (the cooling rate), as a function of θ. *A* denotes the cooling rate due to pair annihilations, while $+-$, *ep*, and *ee* denote the cooling rates due to bremsstrahlung from e^+e^-, *ep*, and $e^{\pm}e^{\pm}$ collisions, respectively. In the four cases n_1n_2 represent n_+n_-, n_+n_-, $(n_+ + n_-)N$, and $n_+^2 + n_-^2$, respectively.

V. CROSS SECTIONS, RATES, AND OPACITIES

The discussion of each process is initiated with a brief description of the cross section (for which the Born approximation is assumed) and its behavior. Coulomb corrections, important near thresholds, are neglected.

a) Photon-Photon Pair Production ($\gamma\gamma \rightarrow e^+e^-$)

The cross section for photon-photon pair production can be found in Jauch and Rohrlich (1976). Expressed in terms of the photon energy x_{CM} in the CM frame, the threshold behavior is

$$\sigma(x_{CM}) = r_e^2 \pi (x_{CM}^2 - 1)^{1/2} \quad (x_{CM} - 1 \ll 1), \tag{23}$$

while the decrease at large photon energies is described by

$$\sigma(x_{CM}) = r_e^2 \frac{\pi}{x_{CM}^2}(2 \ln 2x_{CM} - 1) \quad (x_{CM} \gg 1). \tag{24}$$

The cross section has a maximum at $x_{CM} \approx 1.40$.

The absorption coefficient for photon-photon pair production, $a_{\gamma\gamma}(x, \theta)$ cm^{-1}, for a photon of energy x traversing an isotropic radiation field, was obtained by Gould and Schreder (1966; see Brown, Mikaelian, and Gould 1973 for corrections):

$$a_{\gamma\gamma}(x, \theta) = r_e^2 \pi \int_{1/x}^{\infty} dy n(y, \theta)(xy)^{-2}\phi(xy), \tag{25}$$

where $\phi(s_0 \equiv xy)$ essentially is the cross section averaged over the photon-photon interaction angle.

The optical depth of a uniform region of size R is simply $\tau_{\gamma\gamma}(x, \theta) = a_{\gamma\gamma}(x, \theta)R$. Defining the opacity function

$$O_{\gamma\gamma}(S_i) \equiv \pi \int_{1/x}^{\infty} dy S_i(y, \theta)(xy)^{-2}\phi(xy), \tag{26}$$

the contribution to $\tau_{\gamma\gamma}(x, \theta)$ from the annihilation radiation field is, using equations (8) and (11),

$$\tau_{\gamma\gamma}(x, \theta)_A = \tau_N^2(1 + \tau_T)(z + z^2)O_{\gamma\gamma}(S_A). \tag{27}$$

$O_{\gamma\gamma}(S_A)$ (dashed curves) and $O_{\gamma\gamma}(S_{ep})$ (solid curves) are

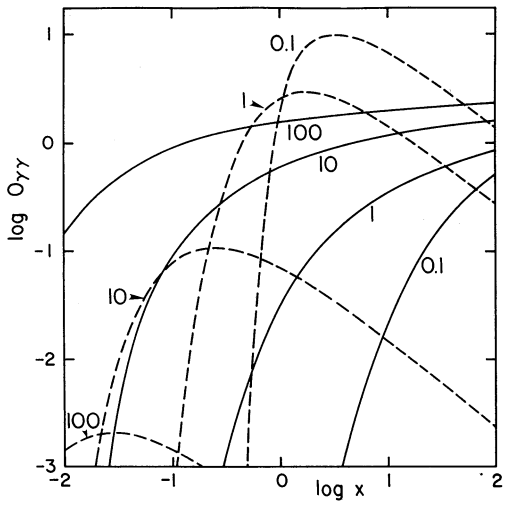

FIG. 2.—The dimensionless opacity function $O_{\gamma\gamma}(S_i)$ as a function of photon energy x at different temperatures θ. The dashed curves represent the opacity function due to annihilation radiation, $O_{\gamma\gamma}(S_A)$, while the solid curves represent the opacity function due to *ep*-bremsstrahlung, $O_{\gamma\gamma}(S_{ep})$. Each curve is labeled by its value of θ.

shown in Figure 2 as a function of temperature and photon energy.

The photon-photon pair production rate, $(\dot{n}_+)_{\gamma\gamma}$ cm^{-3} s^{-1}, is given by

$$(\dot{n}_+)_{\gamma\gamma} = \tfrac{1}{2}c\int_0^\infty dx n(x,\theta)a_{\gamma\gamma}(x,\theta)\,, \qquad (28)$$

where the factor of $\frac{1}{2}$ avoids double counting the interacting photon pairs. Defining the temperature-dependent rate function,

$$P_{\gamma\gamma}(S_i, S_j) \equiv \frac{1}{2}\int_0^\infty dx S_i(x,\theta)O_{\gamma\gamma}[S_j(x,\theta)]\,, \qquad (29)$$

and using equations (11), (25), (26), and (28), the contribution to photon-photon pair production from the annihilation radiation field is

$$\dot{z}_{\gamma\gamma}(n_A, n_A) = t_c^{-1}\tau_N^2(1+\tau_T)^2(z+z^2)^2 P_{\gamma\gamma}(S_A, S_A)\,, \qquad (30)$$

where $\dot{z} \equiv \dot{n}_+/N$ is the production rate in terms of the proton density, and where $t_c^{-1} \equiv cr_e^2 N$. There are nine other rate functions for various combinations of the four radiation fields. In Figure 3 $P_{\gamma\gamma}(S_A, S_A)$ (curve f), $P_{\gamma\gamma}(S_{ep}, S_{ep})$ (curve b), $P_{\gamma\gamma}(S_{+-}, S_{+-})$ (curve a), and $P_{\gamma\gamma}(S_A, S_{+-})$ (curve e) are shown as functions of temperature.

b) Photon-Electron (or Positron) Pair Production ($\gamma e \rightarrow ee^+e^-$)

The threshold behavior for the cross section as a function of the photon energy x as measured in the rest frame of the particle is (Vortruba 1948)

$$\sigma(x) = r_e^2\alpha\frac{3(\pi)^{1/2}}{972}(x-4)^2 \quad (x-4 \ll 1)\,, \qquad (31)$$

while the slow increase at large energies is described by (Borsellino 1947*a*, *b*)

$$\sigma(x) = r_e^2\alpha(\tfrac{28}{9}\ln 2x - \tfrac{218}{27}) \quad (x \gg 1)\,. \qquad (32)$$

The differential cross section was calculated exactly by Haug (1975*a*). The total cross section was then obtained by numerically integrating the differential cross section twice. Haug found that an earlier approximate result by Ghizzetti (1947) and Borsellino (1947*a*, *b*) is correct to within 1.2% for $x > 15$. For $4 \le x \le 15$ we made a numerical fit to Haug's tabulated values of the cross section.

Using Weaver's (1976) results on relativistic reaction rates, the pair production rate is given by

$$(\dot{n}_+)_{ye} = c(n_+ + n_-)[2K_2(1/\theta)]^{-1} \times \int_0^\infty dx n(x,\theta)x^{-2}\int_4^\infty dy y\sigma(y) \times \exp\left[-(x/y + y/x)/2\theta\right]\,. \qquad (33)$$

In a manner similar to equation (28), this rate can also be written as

$$(\dot{n}_+)_{ye} = c\int_0^\infty dx n(x,\theta)a_{ye}(x,\theta)\,, \qquad (34)$$

and from comparing with equation (33) an expression for the absorption coefficient, $a_{ye}(x,\theta)$ cm^{-1}, is easily

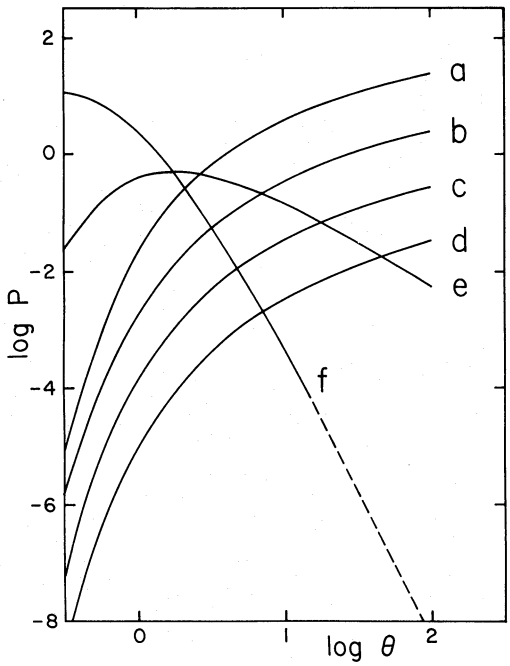

FIG. 3.—The dimensionless pair production rate functions, (*a*) $P_{\gamma\gamma}(S_{+-}, S_{+-})$, (*b*) $P_{\gamma\gamma}(S_{ep}, S_{ep})$, (*c*) $P_{ye}(S_{ep})$, (*d*) $P_{\gamma p}(S_{ep})$, (*e*) $P_{\gamma\gamma}(S_A, S_{+-})$, and (*f*) $P_{\gamma\gamma}(S_A, S_A)$, as a function of temperature θ. The dashed part of curve (*f*) is uncertain as the low energy part of the annihilation spectrum is only approximately known at relativistic temperatures.

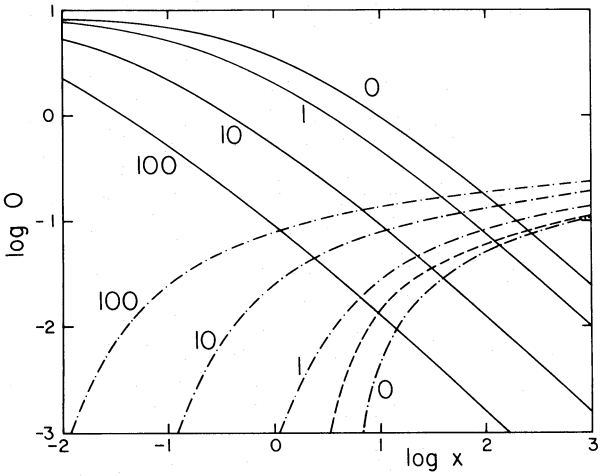

FIG. 4.—The dimensionless scattering function, $O_{cs}(x, \theta)$ is shown by the solid curves as a function of photon energy x at different temperatures θ. Each curve is labeled by its value of θ. The dashed-dotted curves represent the opacity function $O_{ye}(x, \theta)$, while the dashed curve is the opacity function $O_{yp}(x)$. The $\theta = 0$-curves as well as the O_{yp}-curve are just the cross sections for the respective process divided by r_e^2.

obtained. Defining the opacity function $O_{ye}(x, \theta)$ through

$$a_{ye}(x, \theta) \equiv (n_+ + n_-) r_e^2 O_{ye}(x, \theta) \quad (35)$$

and using equations (1) and (7), the optical depth is given by

$$\tau_{ye}(x, \theta) = a_{ye}(x, \theta) R = \tau_N (1 + 2z) O_{ye}(x, \theta) . \quad (36)$$

$O_{ye}(x, \theta)$ is shown in Figure 4 as dashed-dotted curves for different temperatures. It is straightforward to obtain limiting expressions for $O_{ye}(x, \theta)$. Using equation (32) at relativistic temperatures gives

$$O_{ye}(x, \theta) = \alpha \tfrac{28}{9} (\ln 4\eta\theta x - \tfrac{67}{42}) \quad (x \gg \theta^{-1} \wedge \theta \gg 1) , \quad (37)$$

while for nonrelativistic temperatures, $O_{ye}(x, \theta) = \sigma(x)/r_e^2$.

Defining the dimensionless rate function,

$$P_{ye}(S_i) \equiv \int_0^\infty dx S_i(x, \theta) O_{ye}(x, \theta) , \quad (38)$$

and using equations (1), (7), (11), and (33), the pair production rate from the *ep* bremsstrahlung radiation field is

$$\dot{z}_{ye}(n_{ep}) = t_c^{-1} \tau_N (1 + \tau_T)(1 + 2z)^2 P_{ye}(S_{ep}) . \quad (39)$$

Similar expressions are obtained for the other three radiation fields. Figure 3 shows $P_{ye}(S_{ep})$ (curve c).

c) *Photon-Proton Pair Production* ($\gamma p \rightarrow pe^+e^-$)

Racah (1934) obtained the exact cross section as a function of photon energy x. Near threshold the cross section behaves as

$$\sigma(x) = r_e^2 \alpha \frac{2\pi}{3} (x - 2)^3 \quad (x - 2 \ll 1) , \quad (40)$$

while the slow increase at large energy is given by

$$\sigma(x) = r_e^2 \alpha (\tfrac{28}{9} \ln 2x - \tfrac{218}{27}) \quad (x \gg 1) . \quad (41)$$

A useful truncated series expansion of Racah's complicated expression for the cross section with a relative error less than 5×10^{-5} was found by Maximon (1968).

As the protons are nonrelativistic at temperatures of interest, the absorption coefficient is simply $a_{yp}(x) = N\sigma(x)$. The optical depth becomes, using equation (8),

$$\tau_{yp}(x) = a_{yp}(x) R = \tau_N \sigma(x)/r_e^2 \equiv \tau_N O_{yp}(x) , \quad (42)$$

which defines $O_{yp}(x)$. $O_{yp}(x)$ is shown in Figure 4 by the dashed curve.

The photon-proton pair production rate, $(\dot{n}_+)_{yp}$ cm^{-3} s^{-1}, is given by

$$(\dot{n}_+)_{yp} = c \int_2^\infty dx n(x, \theta) a_{yp}(x) . \quad (43)$$

Defining the dimensionless rate function,

$$P_{yp}(S_i) \equiv \int_2^\infty dx S_i(x, \theta) O_{yp}(x, \theta) , \quad (44)$$

and using equation (11), the pair production rate from the *ep* bremsstrahlung radiation field becomes

$$\dot{z}_{yp}(n_{ep}) = t_c^{-1} \tau_N (1 + \tau_T)(1 + 2z) P_{yp}(S_{ep}) . \quad (45)$$

The three other radiation fields give similar expressions. $P_{yp}(S_{ep})$ is shown in Figure 3 (curve d).

d) *Particle-Particle Pair Production* ($ee \rightarrow eee^+e^-$, $ep \rightarrow epe^+e^-$)

The cross sections have so far only been treated in the extreme relativistic limit (see Budnev *et al.* 1975 for references; Kuraev and Lipatov 1975). The general result is

$$\sigma(\gamma) = r_e^2 \alpha^2 \frac{28}{27\pi} (\ln^3 2\gamma - c_2 \ln^2 2\gamma + c_1 \ln 2\gamma + c_0) \quad (\gamma \gg 1) , \quad (46)$$

where γ is the Lorentz factor in the rest frame of one particle (in the *ep* case always the proton) and where $c_2 = 178/28$. For the *ep* case, $c_1 \approx 2.6$ and $c_0 \approx 40$, while in the *ee* case, $c_1 \approx -11$ and $c_0 \approx 100$ (Budnev *et al.* 1975). All contributions to c_0 have not yet been calculated (Kuraev and Lipatov 1975), and, furthermore, c_1 and c_0 differ by a few percent in the *ee* case, depending on whether the initial particles are identical or not. These complications are neglected here as our ignorance is even greater at lower energies. We simply assume that the cross sections depend linearly on γ between the threshold γ_t and some γ_c, above which equation (46) is used. We choose $\gamma_c = 50$ in the *ep* case and $\gamma_c = 90$ in the *ee* case; $\gamma_t = 3$ and 7 for *ep* and *ee* collisions, respectively.

The pair production rate, $(\dot{n}_+)_{ep}$ cm^{-3} s^{-1}, due to *ep*

collisions is obtained by averaging the cross section over the particle distribution, equation (2), which gives

$$(\dot{n}_+)_{ep} = (n_+ + n_-)Nc \int_3^\infty d\gamma f(\gamma)\beta\sigma(\gamma)$$

$$\equiv (n_+ + n_-)Ncr_e^2 P_{ep}(\theta)\,, \quad (47)$$

defining the dimensionless rate function $P_{ep}(\theta)$. Using equations (1) and (7), this expression is rewritten as

$$\dot{z}_{ep} = t_c^{-1}(1 + 2z)P_{ep}(\theta)\,. \quad (48)$$

At extreme relativistic temperatures P_{ep} becomes

$$P_{ep} = \alpha^2 \frac{28}{27\pi}[\ln^3 2\theta + (\tfrac{3}{2}I_1 - c_2)\ln^2 2\theta + (\tfrac{3}{2}I_2 - c_2 I_1 + c_1)\ln 2\theta + \tfrac{1}{2}(I_3 - c_2 I_2 + c_1 I_1 + 2c_0)] \quad (\theta \gg 1)\,, \quad (49)$$

where

$$I_n = \int_0^\infty dz \exp(-z)z^2(\ln z)^n \quad (50)$$

is evaluated to give $I_1 = 3 - 2\gamma_E$, $I_2 = 2.493$, and $I_3 = 3.450$.

Using Weaver's (1976) results, the pair production rate, $(\dot{n}_+)_{ee}$ cm^{-3} s^{-1}, due to *ee* collisions is

$$(\dot{n}_+)_{ee} = \tfrac{1}{2}(n_+ + n_-)^2 c \int_7^\infty d\gamma F(\gamma)\beta\sigma(\gamma)$$

$$\equiv (n_+ + n_-)^2 cr_e^2 P_{ee}(\theta)\,, \quad (51)$$

which defines the dimensionless rate function $P_{ee}(\theta)$. $F(\gamma)$ is given by

$$F(\gamma) = [\theta K_2(1/\theta)]^{-2}\beta\gamma^2(2\gamma_{CM}/\theta)^{-1}K_1(2\gamma_{CM}/\theta)\,. \quad (52)$$

where $\gamma_{CM} = [(\gamma + 1)/2]^{1/2}$. Using equations (1) and (7), equation (51) is rewritten as

$$\dot{z}_{ee} = t_c^{-1}(1 + 2z)^2 P_{ee}(\theta)\,. \quad (53)$$

For reasons similar to those given in § IIIc, the *ee* pair production rate in the very extreme relativistic limit becomes a factor of $\frac{1}{2} \times 2^3$ larger than the *ep* pair production rate. The leading term of P_{ee} is

$$P_{ee} = \tfrac{1}{2}\alpha^2 \frac{28}{27\pi}(2\ln 2\theta)^3 \quad (\theta \gg 1)\,. \quad (54)$$

P_{ep} and P_{ee} are shown in Figure 5. P_{ee} also exceeds P_{ep} at low temperatures, although the rest frame threshold is *larger* for *ee* collisions. This is because the effective threshold in the observer's frame for *ee* collisions is approximately $[(\gamma_t + 1)/2]^{1/2} = 2$, which is *smaller* than the threshold for *ep* collisions.

e) Pair Annihilation ($e^+e^- \rightarrow \gamma\gamma$)

The cross section is given in Jauch and Rohrlich (1976). At nonrelativistic velocities the cross section becomes

$$\sigma(\gamma) = r_e^2 \frac{\pi}{\beta} \quad (\alpha \ll \beta \ll 1)\,, \quad (55)$$

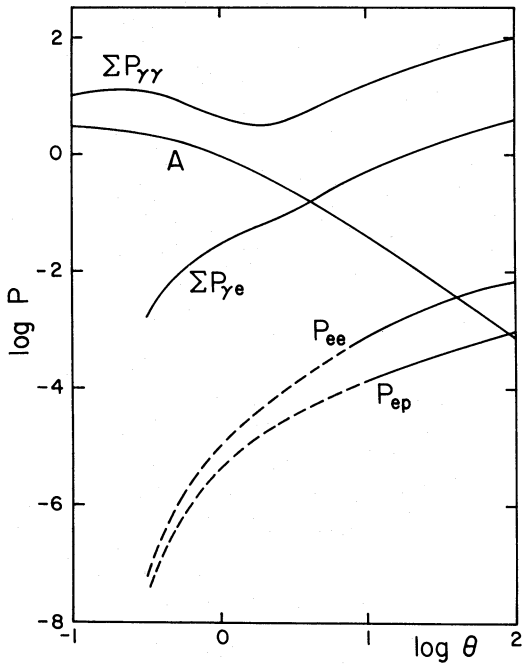

FIG. 5.—The dimensionless pair production rate functions and the dimensionless annihilation rate function, A, as a function of temperature θ. The curves are dashed where the rate functions are uncertain.

while at relativistic energies the cross section decreases as

$$\sigma(\gamma) = r_e^2 \frac{\pi}{\gamma}(\ln 2\gamma - 1) \quad (\gamma \gg 1)\,, \quad (56)$$

where γ is the Lorentz factor in the rest frame of one particle.

The pair annihilation rate, $(\dot{n}_+)_A$ cm^{-3} s^{-1}, is written as (cf. eqs. [51] and [52])

$$(\dot{n}_+)_A = n_+ n_- c \int_1^\infty d\gamma F(\gamma)\beta\sigma(\gamma) = n_+ n_- cr_e^2 A(\theta)\,, \quad (57)$$

which defines the dimensionless rate function $A(\theta)$. Using equations (1) and (7), equation (57) is rewritten as

$$\dot{z}_A = t_c^{-1}(z + z^2)A(\theta)\,. \quad (58)$$

The asymptotic forms of A, $A = \pi$ for $\theta \ll 1$ and $A = (\pi/2)\theta^{-2}\ln(2\eta\theta)$ for $\theta \gg 1$ (Svensson 1982), are combined into an expression that deviates by no more than 2% at all temperatures of interest,

$$A(\theta) = \frac{\pi}{1 + 2\theta^2/\ln(2\eta\theta + 1.3)}\,. \quad (59)$$

The decline of A at relativistic temperatures, as shown in Figure 5, is due to the decreasing cross section at large energies.

f) Three Quantum Annihilation ($e^+e^- \rightarrow \gamma\gamma\gamma$)

The annihilation rate due to three quantum annihilations is a factor of $3\pi/[4\alpha(\pi^2 - 9)] \approx 371$ smaller

than the two quantum annihilation rate at nonrelativistic temperatures (Ore and Powell 1949). At relativistic temperatures the three quantum annihilation rate is expected to increase logarithmically with temperature relative to the two quantum annihilation rate (see Gould 1979 for the corresponding case of double Compton scattering vs. Compton scattering). If so, three quantum annihilation can safely be neglected as an annihilation channel for $\theta < 10^2$.

g) *Compton Scattering* ($\gamma e \rightarrow \gamma e$)

The cross section, given in Jauch and Rohrlich (1976), is constant at low photon energy x (as measured in the rest frame of the particle),

$$\sigma(x) = r_e^2 \frac{8\pi}{3} \quad (x \ll 1) , \tag{60}$$

while at large photon energy (the Klein-Nishina limit) it decreases as

$$\sigma(x) = r_e^2 \frac{\pi}{x} (\ln 2x + \tfrac{1}{2}) \quad (x \gg 1) . \tag{61}$$

The scattering coefficient, $a_{cs}(x)$ cm^{-1}, is given by (cf. eqs. [33] and [34])

$$a_{cs}(x, \theta) = (n_+ + n_-)[2K_2(1/\theta)]^{-1} x^{-2} \times \int_0^\infty dy y \sigma(y) \exp\left[-(x/y + y/x)/2\theta\right] . \tag{62}$$

Defining the scattering function through

$$a_{cs}(x, \theta) \equiv (n_+ + n_-) r_e^2 O_{cs}(x, \theta) , \tag{63}$$

the scattering optical depth becomes, using equations (1) and (7),

$$\tau_{cs}(x, \theta) = a_{cs}(x, \theta) R = \tau_N (1 + 2z) O_{cs}(x, \theta) . \tag{64}$$

$O_{cs}(x, \theta)$ is shown in Figure 4 (solid curves) as a function of photon energy at different temperatures. For relativistic temperatures the Klein-Nishina decline starts at $x \approx \theta^{-1}$. Asymptotic forms for $O_{cs}(x, \theta)$ can easily be derived. At nonrelativistic temperatures, $O_{cs}(x, \theta) = \sigma(x)/r_e^2$, while in the Thomson limit ($x \ll \theta^{-1}$) at relativistic temperatures, $O_{cs}(x, \theta) = 8\pi/3$. Using equation (61) in equation (62) gives, at relativistic temperatures,

$$O_{cs}(x, \theta) = \frac{\pi}{2\theta x} (\ln 4\eta\theta x + \tfrac{1}{2}) \quad (x \gg \theta^{-1} \wedge \theta \gg 1) . \tag{65}$$

The asymptotic opacities given by equations (37) and (65) have been obtained independently by Gould (1982).

VI. OPTICALLY THIN PAIR EQUILIBRIA

a) *The Pair Equilibrium Equation*

The pair density equilibrium equation is obtained by setting the net pair production rate, $\dot{z}$, equal to zero,

$$\dot{z} = \dot{z}_P - \dot{z}_A = 0 . \tag{66}$$

Here $\dot{z}_P$ is the total pair production rate

$$\dot{z}_P = \dot{z}_{\gamma\gamma}(n, n) + \dot{z}_{\gamma e}(n) + \dot{z}_{\gamma p}(n) + \dot{z}_{ee} + \dot{z}_{ep} , \tag{67}$$

$\dot{z}_A$ is given by equation (58), and the photon density n is given by equation (11). The rate $\dot{z}_P$ consists of $4 \times 4 + 4 + 4 + 1 + 1 = 26$ terms, 5 of which are given by equations (30), (39), (45), (48), and (53). Equation (66) can formally be written as a polynomial equation in z,

$$\sum_{i=0}^{I} b_i(\tau_N, \theta) z^i = 0 , \tag{68}$$

where $I = 6$ or 4, depending on whether spatial diffusion is taken into account or not. The coefficients $b_i(\tau_N, \theta)$ are polynomials in τ_N,

$$b_i(\tau_N, \theta) = \sum_{j=0}^{J} d_{ij}(\theta) \tau_N{}^j , \tag{69}$$

where $J = 4$ or 2, depending on whether spatial diffusion is included or not, and where $d_{ij}(\theta)$ are sums of the rate functions defined and calculated in § V.

The equilibrium pair density, n_+, is a function of the three parameters: N, R, and θ. As the general solution of equation (66) can be written as $z = z(\tau_N, \theta)$, the pair density becomes $n_+ = n_+(N, R, \theta) = Nz(\tau_N, \theta)$. There are, however, two limiting cases, where the parameter space of the problem becomes two-dimensional and the pair equilibrium equation reduces to a second-order polynomial equation. One case occurs when $\tau_N \ll 1$ and the solution satisfies $z \ll \tau_N{}^{-1}$. Then the pair density is independent of the radiation field and thus the plasma size R (cf. eqs. [5] and [6]). The other case occurs when $\tau_N \ll 1$ and the solution satisfies $z \gg 1$. Then the pair density is independent of the background proton density N.

In Figure 6 the behavior of $\dot{z}_P$ (dashed curve) and $\dot{z}_A$ (solid curves) are shown schematically for a given

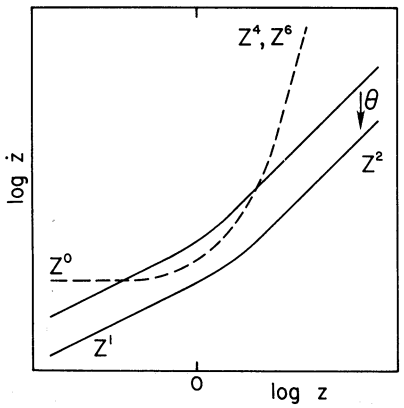

FIG. 6.—The dimensionless total pair production rate, $\dot{z}_P$, is shown schematically by the dashed curve as a function of the dimensionless pair density z. The solid curves represent the dimensionless annihilation rate, $\dot{z}_A$, at two different temperatures θ. (The arrow points in the direction of increasing θ.) At higher temperatures the annihilation rate cannot balance the pair production rate and no equilibrium solutions exist. Different parts of the curves are labeled by their power-law dependence on z.

τ_N as a function of z and θ. As $\dot{z}_P$ increases slowly (for $\theta > 1$) and $\dot{z}_A$ decreases rapidly with θ, there exists a temperature $\theta_c(\tau_N)$ above which pair annihilation cannot balance pair production and no equilibrium solution exists. For $\theta < \theta_c(\tau_N)$ there are two roots, one low-z and one high-z, to equation (66).

b) *The Low-z Case*

For $\tau_N \ll 1$ and $z \ll \tau_N^{-1}$, pair production involving photons is negligible compared to particle-particle pair production, and equation (66) becomes

$$(1 + 2z)^2 P_{ee} + (1 + 2z)P_{ep} - (z + z^2)A = 0 , \quad (70)$$

which can be rewritten as

$$(4P_{ee} - A)z^2 + (4P_{ee} + 2P_{ep} - A)z + P_{ee} + P_{ep} = 0 . \quad (71)$$

The solution of equation (71) is a function of temperature only, and the pair density becomes $n_+ = n_+(N, \theta) = Nz(\theta)$. In Figure 7 $z(\theta)$ is shown as the curve denoted by $\tau_N = 0$. The solution approaches infinity at the temperature, $\theta_{\max}$, where the coefficient of z^2 becomes zero, i.e., when

$$4P_{ee}(\theta_{\max}) = A(\theta_{\max}) . \quad (72)$$

For temperatures larger than $\theta_{\max} \approx 25$ no equilibrium solution is possible. Figure 5 shows that P_{ee} and P_{ep} are much smaller than A for $\theta \ll \theta_{\max}$. Then the solution of equation (71) becomes

$$z = \frac{P_{ee} + P_{ep}}{A} \ll 1 \quad (\theta \ll \theta_{\max}) . \quad (73)$$

The uncertainty of this approximate solution is directly proportional to the uncertainty in P_{ee} and P_{ep} (see § V*d*).

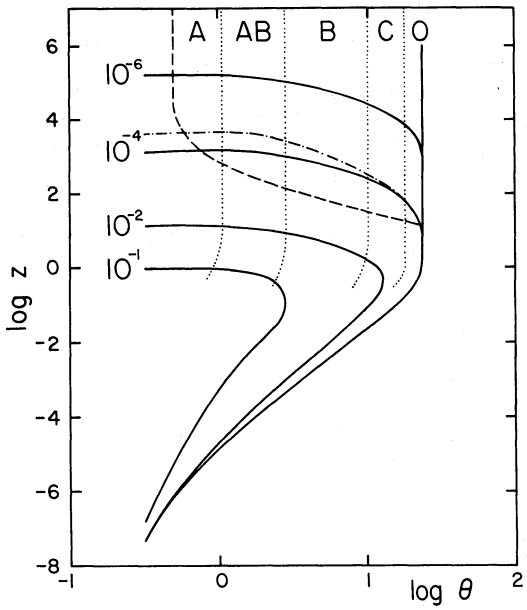

FIG. 7.—The dimensionless equilibrium pair density z is shown as a function of temperature θ by the solid curves. Each curve is labeled by its value of τ_N. Spatial diffusion was not included for the dashed-dotted curve. Above the dashed curve the kinetic energy density of a plasma in pair equilibrium exceeds the rest mass energy density (eq. [86]). The dotted curves outline different pair production regimes. In regions A, AB, and B, pair production is dominated by photon-photon pair production from annihilation photons, from annihilation photons interacting with bremsstrahlung photons, and from bremsstrahlung photons, respectively. In region C, pair production is dominated by photon-particle collisions, while near the $\tau_N = 0$ curve particle-particle collisions predominate.

c) *The High-z Case*

For $\tau_N \ll 1$ and $z \gg 1$, the pair equilibrium equation (66) becomes

$$z^4\tau_N^2(1 + \tau_T)^2 \sum P_{\gamma\gamma} + z^3\tau_N(1 + \tau_T) \sum P_{\gamma e} + z^2 4P_{ee} - z^2 A = 0 , \quad (74)$$

where

$$\sum P_{\gamma\gamma} = P_{\gamma\gamma}(S_A, S_A) + 4P_{\gamma\gamma}(S_{ee}, S_{ee}) + P_{\gamma\gamma}(S_{+-}, S_{+-}) + 4P_{\gamma\gamma}(S_A, S_{ee}) + 2P_{\gamma\gamma}(S_A, S_{+-}) + 4P_{\gamma\gamma}(S_{ee}, S_{+-}) , \quad (75)$$

and

$$\sum P_{\gamma e} = 2P_{\gamma e}(S_A) + 4P_{\gamma e}(S_{ee}) + 2P_{\gamma e}(S_{+-}) . \quad (76)$$

$\sum P_{\gamma\gamma}$ and $\sum P_{\gamma e}$ are shown in Figure 5 and are functions of temperature only. The Thomson scattering optical depth from equation (9) for $z \gg 1$ is simply

$$\tau_T = \frac{16\pi}{3}\tau_N z . \quad (77)$$

Changing the dependent variable in equation (74) from z to τ_T gives a second-order polynomial equation in $\tau_T(1 + \tau_T)$,

$$\sum P_{\gamma\gamma}\tau_T^2(1 + \tau_T)^2 + \frac{16\pi}{3}\sum P_{\gamma e}\tau_T(1 + \tau_T) + \left(\frac{16\pi}{3}\right)^2(4P_{ee} - A) = 0 . \quad (78)$$

The solution of equation (78) is a function of temperature only. Then $z = (3/16\pi)\tau_T(\theta)/\tau_N$, and z scales as τ_N^{-1}, as Figure 7 shows. The physical pair density becomes, using equations (8) and (77),

$$n_+(R, \theta) = \frac{3}{16\pi}\frac{\tau_T(\theta)}{r_e^2 R} = 7.5 \times 10^{23} R^{-1}\tau_T(\theta) \text{ cm}^{-3} \quad (n_+ \gg N) . \quad (79)$$

scaling as R^{-1} as shown in Figure 8. The solution approaches zero at $\theta_{\max}$, where the last term in equation (78) becomes zero (cf. eq. [72]).

In the high-z case, pair production is caused by both particles and photons. In Figure 7 the dotted curves show where different pair production mechanisms dominate (see figure text). For $\theta < 10$, photon-photon

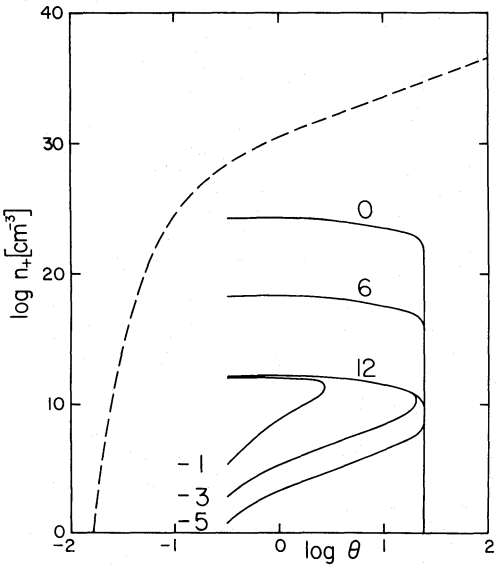

FIG. 8.—The physical pair density n_+ as a function of temperature θ. The high-z solutions (for $\tau_N \ll 1$) are shown as solid curves for log R(cm) equal to 0, 6, and 12. For the last case the complete solution curves are shown for log τ_N equal to -1, -3, and -5. The dashed curve represents the pair density in thermodynamic equilibrium (eq. [87]).

pair production dominates. Then the solution of equation (78) becomes

$$\tau_T(1+\tau_T) = \frac{16\pi}{3}\left(\frac{A}{\sum P_{\gamma\gamma}}\right)^{1/2} \quad (\theta \ll \theta_{\max}) . \qquad (80)$$

Figure 5 shows that $A/\sum P_{\gamma\gamma} \approx 0.20$ and thus $\tau_T \approx 2.3$, approximately independent of temperature for $\theta < 2$. At higher temperatures τ_T decreases. The weak maximum in τ_T ($\propto z \propto n_+$) near $\theta \approx 1$ may disappear when Comptonization and marginally important processes are properly accounted for.

The dashed-dotted curve in Figure 7 shows that neglecting spatial diffusion increases the result by a factor of 3. As $\tau_T > 0.4$ for $\theta < 10$, Comptonization is also expected to be important. Comptonization acts similarly to spatial diffusion in being a photon density-enhancement mechanism (at photon energies of order θ). Increasing the photon density and thus the pair production rate lowers the high-z root (see Fig. 6). Including Comptonization would only lower τ_T and reduce the importance of the effect. Spatial diffusion and Comptonization, therefore, work as self-regulating mechanisms, keeping the solution $\tau_T(\theta)$ at a value of order unity. Thus, Comptonization is not expected to lower the solution curves by more than a factor of 3.

For $\theta < 2$ the density of *pair producing* photons is dominated by annihilation photons. By noticing that the generation rate of annihilation photons, $(\dot{n}_\gamma)_A$, is twice the annihilation rate, $(\dot{n}_+)_A$, and using equations (1), (5)–(8), (57), (77), and (80), the annihilation photon density, $(n_\gamma)_A$, in terms of the total particle density becomes

$$\frac{(n_\gamma)_A}{n_+ + n_-} = A\left(\frac{A}{\sum P_{\gamma\gamma}}\right)^{1/2} , \qquad (81)$$

which is about 1 for $\theta = \frac{1}{3}$ and decreases for larger θ. Note that the result is independent of whether spatial diffusion is included or not.

The results in § V and Figures 2 and 4 show that photon-photon absorption due to annihilation photons at $\theta < 2$ is the only important absorption process. Equations (27) and (80) give

$$\frac{\tau_{\gamma\gamma}(x,\theta)}{\tau_T(\theta)} = \frac{3}{16\pi}\left(\frac{A}{P_{\gamma\gamma}}\right)^{1/2} O_{\gamma\gamma}[S_A(x,\theta)] . \qquad (82)$$

Evaluating equation (82) for $\theta = 1$ at photon energy $x \approx 2$, where the annihilation spectrum peaks, gives $\tau_{\gamma\gamma} \approx 0.08\tau_T \approx 0.18$. The effective absorption optical depth, as discussed by Rybicki and Lightman (1979), is enhanced by the prolonged pathway due to spatial diffusion giving $\tau_{\rm eff} \approx [\tau_{\gamma\gamma}(\tau_{\gamma\gamma} + \tau_T)]^{1/2} \approx 0.3\tau_T \approx 0.7$ for the case considered above (neglecting Klein-Nishina corrections). Comptonization will, when included, make τ_T and thus $\tau_{\rm eff}$ smaller. On the other hand, photon absorption will lower the pair producing photon density and the pair production rate, thus raising the equilibrium z-value (see Fig. 6), τ_T and $\tau_{\rm eff}$. The net effect of including photon absorption and Comptonization is difficult to estimate, and a detailed calculation is needed to determine the behavior of the high-z root at $\theta < 2$. At larger temperatures absorption effects are negligible.

d) Properties of the General Solutions

For $\tau_N \geq 10^{-4}$, equation (66) must be used to determine the equilibrium pair density. The solutions are shown in Figures 7 and 8. The critical temperature $\theta_c(\tau_N)$, beyond which there are no equilibrium solutions, deviates by less than 7% from $\theta_{\max}$ for $\tau_N \lesssim 10^{-4}$ and decreases rapidly with increasing τ_N for $\tau_N > 10^{-4}$. Photon-photon processes dominate the pair production for $\tau_N = 10^{-1}$ and $\theta > \frac{1}{3}$. The model, however, breaks down at $\tau_N \approx 10^{-1}$, where Comptonization and absorption processes need to be included.

The total power, Λ, emitted per unit volume (the cooling rate) from equilibrium pair plasmas is shown in Figure 9, as is the cooling rate for coronal equilibrium at temperatures $\theta < 10^{-2}$ (Raymond, Cox, and Smith 1976). The dotted curve shows the cooling rate one would obtain by setting $z = 0$, thereby completely neglecting the existence of pair producing processes. The cooling curves rise sharply near $\theta_{\max}$, and large heating rates are needed to maintain large equilibrium pair densities. Including the effects of Comptonization would make the cooling on the high-z branches even larger.

To study the stability of the solutions requires a more realistic treatment of the plasma. Nevertheless, assuming

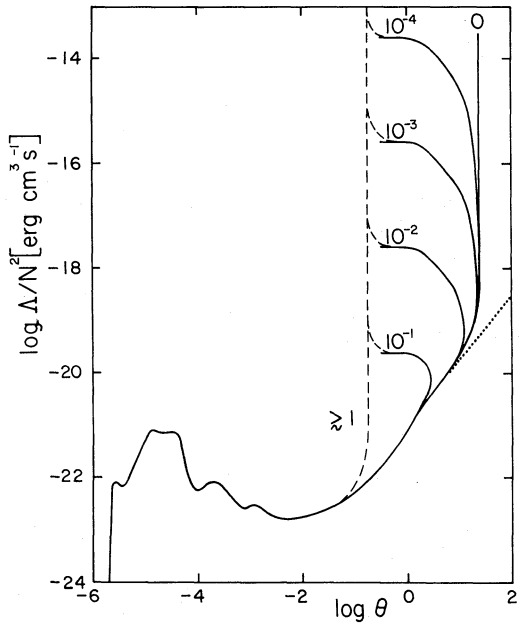

FIG. 9.—The total power emitted per unit volume, Λ (the cooling rate), divided by the square of the proton density, N, as a function of temperature θ. At small temperatures, $\theta < 10^{-2}$, the cooling rate is taken from the results of Raymond, Cox, and Smith (1976). The dotted curve represents the cooling rate if there were no pairs present ($z = 0$). The solid curves show the cooling rates from an optically thin plasma in pair equilibrium. Each curve is labeled by its value of τ_N. The dashed curve represents the cooling rate expected from an optically thick plasma in pair equilibrium.

a static situation, conservation of pairs and energy demand

$$\frac{dz}{dt} = \dot{z}_P(z, \theta) - \dot{z}_A(z, \theta)\,, \tag{83}$$

and

$$\frac{d\epsilon}{dt} = H(z, \theta) - \Lambda(z, \theta)\,, \tag{84}$$

where

$$\epsilon(z, \theta) = Nmc^2(1 + 2z)[K_1(1/\theta)/K_2(1/\theta) + 3\theta] \tag{85}$$

is the pair energy density and $H(z, \theta)$ ergs cm^{-3} s^{-1} is the heating rate. For equilibrium solutions $H = \Lambda$. Equations (83) and (84) are rewritten to form a set of two ordinary differential equations for z and θ. The stability of the equilibrium solutions can be analyzed using the method outlined by Pars (1965). For H independent of z or θ, only the high-z solutions for $\theta < 2$ are unstable. The solutions for $\theta < 2$ in a more detailed treatment may however be stable. If $H \propto z^2$, then $d\epsilon/dt = 0$ for $z \gg 1$, as $\Lambda \propto z^2$ for $z \gg 1$ (see § III), and the plasma evolves isothermally. Figure 6 shows that the high-z solutions are unstable to isothermal z perturbations. In realistic cases H also depends on temperature, and the actual heating mechanism must be specified before the stability of the high-z roots can be determined. Finally, note that the radiation field has been assumed to adjust instantaneously to changed conditions. This is only marginally true on the high-z branch, on which the radiation field is of importance.

The plasma considered here is assumed to be confined. A necessary condition for gravitational confinement, even in a relativistic potential (near a neutron star or a black hole), is that the kinetic energy density of the plasma is smaller than the rest mass energy density. The corresponding constraint on z becomes

$$z < \frac{1}{2}\left[\frac{m_p/m - \frac{3}{2}\theta}{K_1(1/\theta)/K_2(1/\theta) + 3\theta - 2} - 1\right], \tag{86}$$

where m_p is the proton rest mass. For $1 \ll \theta \ll m_p/m$, the inequality simplifies to $z < m_p/(6\theta m)$. Equilibrium plasmas above the dashed line in Figure 7 are not confined, unless some additional confinement mechanism is operating, such as magnetic confinement suggested by Cavallo and Rees (1978) and Ramaty *et al.* (1980) in the case of optically thick pair plasmas. The momentum transfer from internally generated photons to pairs during photon escape counteracts any confinement mechanism. Finally, it should be noted that the Eddington luminosity for an accreting pair plasma can be decreased by up to a factor of m_p/m.

e) Comparison with Other Work

BK included only particle-particle pair production (the low-z case, § VI*b*) and thus solved equation (71). BK's result is in good agreement with ours, although BK obtained $\theta_{\max} \approx 40$ using a less accurate reaction rate P_{ee}.

The low-z solution to Stoeger's (1977) pair equilibrium equation for $\tau_N = 10^{-2}$ is a factor of 10^7 smaller than ours. The difference has three main reasons: (i) all important processes were not included in Stoeger's work; (ii) the reaction rate $P_{\gamma\gamma}$ calculated by Stoeger is a factor of 10^4 too small; and (iii) Stoeger's photon escape time $t_{\rm esc} = R\tau_T/c$ is only valid for $\tau_T > 1$.

After the completion of the present work, a preprint from Lightman (1982) appeared which independently extended the work of earlier authors in a way similar to ours. That paper considered relativistic temperatures, $\theta > 3$, and used relativistic approximations of the reaction rates (calculated to logarithmic accuracy and differing from ours by up to factors of 4). Lightman, however, included Comptonization, using an approximate relativistic theory developed by Lightman and Band (1981). As argued in § VI*c*, this has a self-regulating effect, decreasing the high-z roots somewhat. The qualitative aspects of Lightman's solutions for $z \gg 1$ are similar to ours, although there are differences by factors of 2 or 3. The behavior indicated in Lightman's Figure 1, where for $\tau_N \approx 10^{-3}$–10^{-4} the low-z root becomes of order unity for $\theta \approx 3$–10, is inconsistent with the low-z root of Lightman's pair equilibrium equation, where $z \ll 1$ for the same parameters. Note that Lightman expresses the photon energy in units of kT, that Lightman's τ_N parameter is a factor of $8\pi/3$ larger than ours, and that Lightman solves the pair equilibrium equation for $y = z - 1$.

VII. OPTICALLY THICK PAIR EQUILIBRIA

For a given R, all solution curves join a unique curve $n_+(\theta)$ independent of the background proton density N (or equivalently τ_N), as shown in Figure 8 for $R = 10^{12}$ cm. Although this unique solution curve (for a given R) is somewhat uncertain for $\theta < 2$ and has not been determined for $\theta < \frac{1}{3}$, some qualitative considerations can be made.

If the temperature θ is smaller than $\frac{1}{3}$, Compton recoil removes annihilation photons from the annihilation peak, and the pair production rate becomes smaller. Photon-photon absorption and Compton recoil then work together to cause an increase in the equilibrium pair density (see § VIc). Reverse absorption processes (see Table 1) become important and the state of the plasma becomes independent of the size R. The solution curve, along which $n_\gamma(x \gtrsim 1) \approx n_+$, reaches a minimum temperature $\theta_{\min} \approx \frac{1}{10}$–$\frac{1}{3}$ before joining the thermodynamic equilibrium curve (the dashed curve in Fig. 8), where all processes are balanced by their reverse processes. In a pair dominated plasma ($n_+ \gg N$), the thermodynamic equilibrium pair density is given by (Landau and Lifshitz 1969)

$$n_+(\theta) = \frac{1}{\pi^2 \lambda\!\!\!^{-3}} \int_1^\infty d\gamma \frac{\beta\gamma^2}{\exp(\gamma/\theta) + 1}, \qquad (87)$$

where $\lambda\!\!\!^{-}$ is the Compton wavelength. Setting $n_+(R, \theta_{\min})$ from equation (79) equal to $n_+(\theta_{\min})$ from equation (87) gives $R \approx 2 \times 10^{-4}$ cm for $\theta_{\min} = \frac{1}{3}$. $\theta_{\min}$ is expected to be a weak function of R for $R \gg 10^{-4}$ cm. For smaller R, three-body absorption processes become important before the solution curve reaches $\theta = \frac{1}{3}$, and $\theta_{\min}$ is expected to be a strong function of R.

As discussed in § VId, $\theta_c(\tau_N)$ decreases rapidly with increasing τ_N. Thus, there exists a τ_c (which may depend on N and R) of order unity such that $\theta_c(\tau_c) = \theta_{\min}$. For $\tau_N > \tau_c$ the equilibrium pair density is expected to increase monotonically with temperature and to join the unique solution curve at $\theta \approx \theta_{\min}$ as soon as n_+ becomes much larger than N. The only equilibrium state at $\theta > \theta_{\min}$ for a plasma with $\tau_N > \tau_c$ is the thermodynamic equilibrium state, as conjectured by BK.

The expected behavior of the total power emitted per unit volume for optically thick pair plasmas are shown in Figure 9 as dashed lines. Note that the total cooling rate from the plasma region is not simply given by $\Lambda \times$ (volume), but it is reduced by absorption processes.

VIII. GENERAL DISCUSSION AND SUMMARY

The cooling curves in Figure 9 show that steady plasmas are kept at three characteristic temperatures, $T \approx T_4 \equiv 10^4$ K, $\theta_{\min}$, and $\theta_{\max}$, over a wide range of heating rates. The temperature T_4 is related to the solution of the Dirac equation for a Coulomb field. The energy gap between the two lowest energy levels is $3\alpha^2 mc^2/8$, while the ionization energy is $\alpha^2 mc^2/2$. $\theta_{\min}$ is related to the solution of the Dirac equation in vacuum, where there is a minimum energy gap of $2mc^2$ between negative and positive energy levels. Finally, $\theta_{\max}$ is a consequence of the fact that for two body processes with two final states, such as pair annihilation, phase space restrictions due to energy-momentum conservation causes the cross section to decrease at relativistic energies.

At T_4 an increased heating rate will maintain a higher excitation and ionization level, without raising the temperature by much, while at $\theta_{\min}$ and $\theta_{\max}$ an increased heating rate will maintain a higher equilibrium pair density. The significant difference is that low-temperature plasmas can reach complete ionization, while in high-temperature plasmas the equilibrium pair density, possible to excite from the vacuum, is only limited by reaching thermodynamic equilibrium. This is the cause for the large range of heating rates for which the temperature will be kept at $\theta_{\min}$ or $\theta_{\max}$.

The temperatures $\theta_{\min}$ and $\theta_{\max}$ could play as important a role in high-energy plasmas as the temperature T_4 does in interstellar plasmas. However, necessary heating rates are only available near compact objects, such as black holes and neutron stars. There the dynamical time scales are short and a strongly heated pair plasma may not be in either thermal balance or pair equilibrium. Nevertheless, even nonsteady pair plasmas, during their evolution, could pass through a state of quasi-steady equilibrium. Such is the case for scenario II in Cavallo and Rees (1978), where the optically thick pair plasma during its annihilation phase evolves down the $\theta_{\min}$-branch (see § VII) until $\tau_T \approx 1$.

Neither the heating mechanisms nor the thermal balance equation were considered in this work. To do this one must specify the macroscopic environment of the plasma region, in which case it may be necessary to treat the problem as time dependent and inhomogeneous. Two such examples are thermonuclear flashes on the surface of neutron stars to model gamma-ray bursts and gas accretion onto massive black holes to model quasar continua. Furthermore, it will be necessary to include effects of magnetic fields and soft-photon generation. In particular, Comptonized soft photons may play a major role in determining the properties of realistic semi-relativistic plasmas.

We summarize the obtained overall picture of possible pair equilibria:

For $\tau_N < \tau_c$, where τ_c is of order unity, there exist three temperature regions. At $\theta < \theta_{\min}$, where $\theta_{\min} \approx \frac{1}{10}$–$\frac{1}{3}$, there is only one (optically thin) solution to the pair equilibrium equation. For $\theta_{\min} < \theta < \theta_c(\tau_N)$ there are three equilibrium solutions: (i) the optically thin case, (ii) the marginally optically thick case ($\tau_T \approx 1$), and (iii) the thermodynamic equilibrium case. The equilibrium solutions (i) and (ii) were determined quantitatively in the temperature range $\theta > \frac{1}{3}$. $\theta_c(\tau_N)$ is a decreasing function of τ_N with a maximum value $\theta_{\max} \approx 25$. For $\theta > \theta_c(\tau_N)$ thermodynamic equilibrium is the only pair equilibrium state. Finally, for $\tau_N > \tau_c$ there is only one equilibrium pair density at any temperature.

The author thanks William G. Mathews, George R. Blumenthal, and Claes-Ingvar Bjornsson for helpful discussions. This work was supported mainly by a Swedish doctoral fellowship and partly by NSF grant AST 80-08246 and the Board of Studies in Astronomy and Astrophysics, University of California, Santa Cruz.

REFERENCES

Alexanian, M. 1968, *Phys. Rev.*, **165**, 253.
Baĭer, V. N., Fadin, V. A., and Kroze, V. A. 1968, *Soviet Phys.—JETP*, **26**, 1238.
Baity, W. A., Rothschild, R. E., Worrall, D. M., Peterson, L. E., Primini, F. A., Levine, A. M., and Lewin, W. H. G. 1981, *Bull. AAS*, **12**, 795.
Bignami, G. F., *et al.* 1981, *Astr. Ap.*, **93**, 71.
Bisnovatyi-Kogan, G. S., Zel'dovich, Ya. B., and Sunyaev, R. A. 1971, *Soviet Astr.—AJ*, **15**, 17 (BK).
Borsellino, A. 1947*a*, *Nuovo Cimento*, **4**, 112.
———. 1947*b*, *Rev. Univ. Nac. Tucumán*, **A6**, 7.
Brown, R. W., Mikaelian, K. O., and Gould, R. J. 1973, *Ap. Letters*, **14**, 203.
Budnev, V. M., Ginsburg, I. F., Meledin, G. V., and Servo, V. G. 1975, *Phys. Rept.*, **15**, 183.
Cavallo, G., and Rees, M. J. 1978, *M.N.R.A.S.*, **183**, 359.
Frank-Kamenetskii, D. A. 1962, *Physical Processes in Stellar Interiors* (Jerusalem: Israel Program for Scientific Translations).
Ghizzetti, A. 1947, *Rev. Univ. Nac. Tucumán*, **A6**, 37.
Gould, R. J. 1979, *Ap. J.*, **230**, 967.
———. 1980, *Ap. J.*, **238**, 1026.
———. 1981*a*, *Ap. J.*, **243**, 677.
———. 1981*b*, *Phys. Fluids*, **24**, 102.
———. 1982, *Ap. J.*, **254**, 755.
Gould, R. J., and Schreder, G. P. 1966, *Phys. Rev.*, **155**, 1404.
Haug, E. 1975*a*, *Zs. Naturforschung*, **30a**, 1099.
———. 1975*b*, *Zs. Naturforschung*, **30a**, 1546.
Jauch, J. M., and Rohrlich, F. 1976, *The Theory of Photons and Electrons*, 2d ed. (New York: Springer-Verlag).
Joseph, J., and Rohrlich, F. 1958, *Rev. Mod. Phys.*, **30**, 354.
Kuraev, E. A., and Lipatov, L. N. 1975, *Soviet J. Nucl. Phys.*, **20**, 58.
Kylafis, N. D., and Lamb, D. Q. 1982, *Ap. J. Suppl.*, **48**, in press.
Landau, L. D., and Lifshitz, E. M. 1969, *Statistical Physics*, 2d ed. (New York: Pergamon).
Lightman, A. P. 1982, *Ap. J.*, **253**, 842.
Lightman, A. P., and Band, D. L. 1981, *Ap. J.*, **251**, 713.
Maximon, L. C. 1968, *J. Res. NBS*, **72B**, 79.
Maxon, S. 1972, *Phys. Rev.*, **A5**, 1630.
Mazets, E. P., Golenetskii, S. V., Aptekar', R. L., Gur'yan, Yu. A., and Il'inskii, V. N. 1981, *Nature*, **290**, 378.
Ore, A., and Powell, J. L. 1949, *Phys. Rev.*, **75**, 1696.
Pars, L. A. 1965, *A Treatise on Analytical Dynamics* (London: Heinemann).
Quigg, C. 1968, *Ap. J.*, **151**, 1187.
Racah, G. 1934, *Nuovo Cimento*, **11**, 477.
Ramaty, R., Bonazzola, S., Cline, T. L., Kazanas, D., Mészáros, P., and Lingenfelter, R. E. 1980, *Nature*, **287**, 122.
Ramaty, R., and Mészáros, P. 1981, *Ap. J.*, **250**, 384.
Raymond, J. C., Cox, D. P., and Smith, B. W. 1976, *Ap. J.*, **204**, 290.
Rybicki, G. B., and Lightman, A. P. 1979, *Radiative Processes in Astrophysics* (New York: Wiley-Interscience).
Stickforth, J. 1961, *Zs. Phys.*, **164**, 1.
Stoeger, W. R. 1977, *Astr. Ap.*, **61**, 659.
Svensson, R. 1982, *Ap. J.*, **258**, 321.
Vortruba, V. 1948, *Phys. Rev.*, **73**, 1468.
Weaver, T. A. 1976, *Phys. Rev.*, **A13**, 1563.
Zdziarski, A. A. 1980, *Acta Astr.*, **30**, 371.

ROLAND SVENSSON: European Southern Observatory, Karl-Schwarzschild-Strasse 2, D-8046 Garching bei München, West Germany